Contents

Table of Figures

General introduction and motivation

In the field of molecular switches, spin crossover (SCO) compounds present a special interest due to the wide range of their potential applications. These transition metal complexes exhibit reversible switching between the so-called low spin (LS) and high spin (HS) electronic configurations [1-3]. The conversion between these two states can be triggered by various external stimuli such as temperature, pressure, light or X-ray irradiation, an intense magnetic field or the inclusion of guest molecules. The two spin states can then be distinguished by their different magnetic, optical, mechanical, spectroscopic and structural properties. The changes associated with the spin transition can propagate in a cooperative manner [4], which can produce hysteresis phenomena even at room temperature. An appealing aspect of the spin transition is that the switching of the electronic configuration can occur on a sub-ps scale [5], which can translate into THz scale processing rate. From the technological point of view SCO materials have been proposed for numerous applications ranging from displays [6], memory devices [7], pressure and temperature sensors [8], gas sensors [9], nanothermometers [10], optoelectronic devices [11] and actuators [12].

Considering the vast applicability of these materials, several research groups have recently embarked on the study of electrical properties of SCO compounds including the possibility of their addressing by electrical field and/or current. The use of electrical stimuli to control (read/write) the spin-state of the system would provide a great advantage to other stimuli such as temperature or pressure due to a faster dynamics (less inertia), easier size reduction and better compatibility with current technology. Indeed, while the optical, vibrational and magnetic properties have been extensively studied for these compounds, their electrical properties remain mostly unexplored.

Recently, several encouraging results indicated a spin state dependence of the charge transport in SCO molecules and nanoparticles. Nevertheless, in the majority of these studies the fabrication and the characterization of these devices are rather inadequate leading to several uncertainties in the interpretation of their results, in particular giving rise to a strong discrepancy with the bulk

properties. However, these results are extremely important from a fundamental point of view, pointing out exciting perspectives for applications in the fields of spintronics and molecular electronics. The pioneering result in electrical characterization of SCO materials has been the detection of the thermal variation of the real part of the dielectric permittivity, exhibiting a hysteretic and photoswitchable behavior in the same manner as the magnetic susceptibility [13,14]. In this case the imaginary part of the permittivity, which is related to the electrical conductivity did not exhibit any spin state dependence. In order to overcome this drawback, by improving the conductivity of SCO materials, a new approach has been proposed by using the co-crystallization of molecular conductors and SCO complexes to form "conductor-SCO hybrids" [15]. This approach lead to an enhancement by several orders of magnitude the low conductivity of pure SCO materials, leading in some cases [16,17] to a rather convincing spin state dependence with the LS state being more conductive than the HS state dependence of the electrical conductivity. The first report of a significant conductivity modulation due to spin crossover has been found in the pure $[Fe(HB(pyrazolyl)_3)_2]$ complex, however the complicated interplay between the structural and electronic degrees of freedom lead to irreversible changes of the physical properties after the first cycle [18,19]. The unambiguous spin state dependence of the dc electrical conductivity has been reported on powder and nanoparticle samples of the compound $[Fe(Htrz)_2(trz)](BF_4)$ (Htrz = 1H-1,2,4-triazole). The dc conductivity presented a clear hysteresis loop, with a more conductive LS state, highlighting the interplay between the spin transition temperatures and the activation parameters [20]. The transport properties of SCO materials at the single molecule or single nanoparticle level have been studied in several recent papers, with promising results towards the application of these materials in molecular electronics and spintronics [21-24]. In each of these papers current-voltage characteristics have been used to characterize the molecular devices, however the results are rather uncertain due to the fact that the change in current might have other origins than the spin transition. The interpretation of these results are rather speculative due to the fact that different physical properties observed on a macroscopic ensemble of SCO particles has been extrapolated to single molecules and single nanoparticles.

In this context, the present thesis aims at presenting a more thorough analysis on the transport properties of SCO materials as well as their integration into micro- and nanoelectronic devices. Broadband dielectric spectroscopy has been used to reveal the **quasi-static and dynamic**

electrical properties of SCO materials at a macroscopic level. Micrometric rods were integrated in a well-controlled manner between interdigitated gold electrodes in order to obtain **microelectronic devices** and to study their behavior in variable temperature, under light irradiation and the effect of an external electric field. The robustness and the stability of the sample and the electronic device have been also studied. The SCO based electronic devices have been scaled down to nanometric scale, obtaining a series of **thin film nanoelectronic devices**, which have been thoroughly characterized. All the electrical measurements are complemented by chemical and structural analysis of the compounds.

The manuscript is organized as follows:

The thesis begins with a general introduction and motivation.

Chapter 1 is structured in two main sections consisting of an introduction in the SCO phenomena, the physical principles behind the transition and the stimuli that induce the spin crossover followed by a short description of the techniques used to detect the spin transition. The second part of this chapter consists of an exhaustive review of the achievements in the field of electrical and charge transport properties of SCO materials organized in three main categories: electrical properties of macroscopic samples, micro- and nanoscale devices and single molecule devices.

Chapter 2 starts with a short explanation of the working principle and the theory behind the broadband dielectric spectroscopy. Based on previous results from the team [20,25] this technique has been used to analyze the static and dynamic electrical properties of the $[Fe(Htrz)_2(trz)](BF_4)$ complex and the Zn diluted series of the same compound as well as the role of the iron center in the charge transport mechanism. Various electric quantities that represent different facets of the charge carrier dynamics in these systems like conductivity, permittivity and electrical modulus have been analyzed. The electrical study is completed by optical and spectroscopic characterization of the samples in order to accurately determine the effect of Zn dilution on the structure, morphology as well as on the charge transport properties.

The fabrication of a microelectronic device is presented in **Chapter 3**, were micrometric sized rods of $[Fe(Htrz)_2(trz)](BF_4)$ have been organized by dielectrophoresis between interdigitated gold electrodes. Before the integration of the sample in the device, the robustness of the SCO

phenomena has been tested through a considerable amount of thermal switches. The influence of different solvents on the spin transition has been also tested. Optimal parameters for dielectrophoresis were determined experimentally for this particular system. Then the effect of temperature, light irradiation and applied bias on the device has been investigated. An exceptional breakthrough towards the implementation of real spintronic devices would be the control of the spin state using an electrical stimuli, therefore, the effect of the electric field has been studied carefully. The results were then analyzed using a simple model based on the interaction between the electric field and the electric dipole moment of spin crossover complexes.

Chapter 4 describes an alternative approach for charge transport measurements in the tunneling regime based on robust, well-reproducible large-area vertical devices with thin SCO spacer layers. Electronic devices in vertical configuration were fabricated with the $[Fe(bpz)_2(phen)]$ (bpz = dihydrobis(pyrazolyl)borate and phen = 1,10-phenantroline) complex. We have chosen this complex because it is well known to give high quality films. We evaporated thin films of this complex with thickness of 10 nm, 30 nm and 100 nm. This approach allowed to probe the spin-state switching in the SCO layer by optical means while detecting the associated resistance changes both in the tunneling (thin junction) and injection-limited (thick junction) regimes. The high current intensity in the devices provided also possibility for mechanistic studies by means of temperature- and frequency-dependent dielectric spectroscopy. Electrical measurements have been completed by optical, magnetic, crystallographic, and spectroscopic measurements of the SCO complex in powder, thin film and in sandwich configuration, providing a complete study of the material and nanoelectronic devices.

The manuscript ends with general conclusions and perspectives.

Chapter 1: Introduction

This chapter consists of an introduction to the spin crossover phenomenon, presenting first the electronic and the thermodynamic phenomena that governs the spin transition, followed by the short presentation of the main stimuli that can be used to induce the spin transition and the most common detection techniques. The second part of this chapter provides a review of the research about the electrical and charge transport properties of spin crossover complexes.

1.1 Spin crossover phenomenon

In the framework of the crystal field theory it is shown that some materials containing transition metals in the electronic configuration $3d^n$ ($4 < n < 7$), can exhibit two fundamental electronic states depending on the crystal field strength, namely the low spin state (LS) and the high spin state (HS). The effect of the octahedral field causes the energy levels of the d orbitals to split into two energy levels: a first level t_{2g} containing three non-bonding orbitals with triple degeneracy (d_{xy}, d_{yz}, d_{zx}), and a second level, e_g^*, containing two anti-bonding orbitals with double degeneracy (d_{z^2}, $d_{x^2-z^2}$) as shown in Figure 1.1. These two energy levels are separated by an energy gap $\Delta = 10$ Dq, that characterizes the ligand field strength. This gap depends on the nature of the metal ion, of the surrounding ligands and the metal-ligand length. For the systems containing more than one d electron, the electron-electron repulsion (pairing energy Π) has to be also considered in the same time as the ligand field. In the case of Fe^{II} with d^6 electronic configuration, two extreme cases can be imagined as a function of ligand field strength (Figure 1.1), giving rise two fundamental states $^1A_1$ and $^5T_2$:

- When $\Pi > 10$ Dq (weak crystalline field): the d electrons occupy the two energy levels t_{2g} and e_g^* in accordance with Hund's law of the maximum parallel spins. The resulting total spin is S = 2 and the electronic configuration energetically favorable is the paramagnetic HS state $^5T_2$ $(t_{2g})^4 (e_g^*)^2$.

- When $\Pi < 10$ Dq (strong crystalline field): the electrons are paring on the orbitals with the lowest energy, t_{2g}, ignoring Hund's law. The resulting spin is S = 0 and the complex is found in the diamagnetic LS state $^1A_1$ $(t_{2g})^6$.
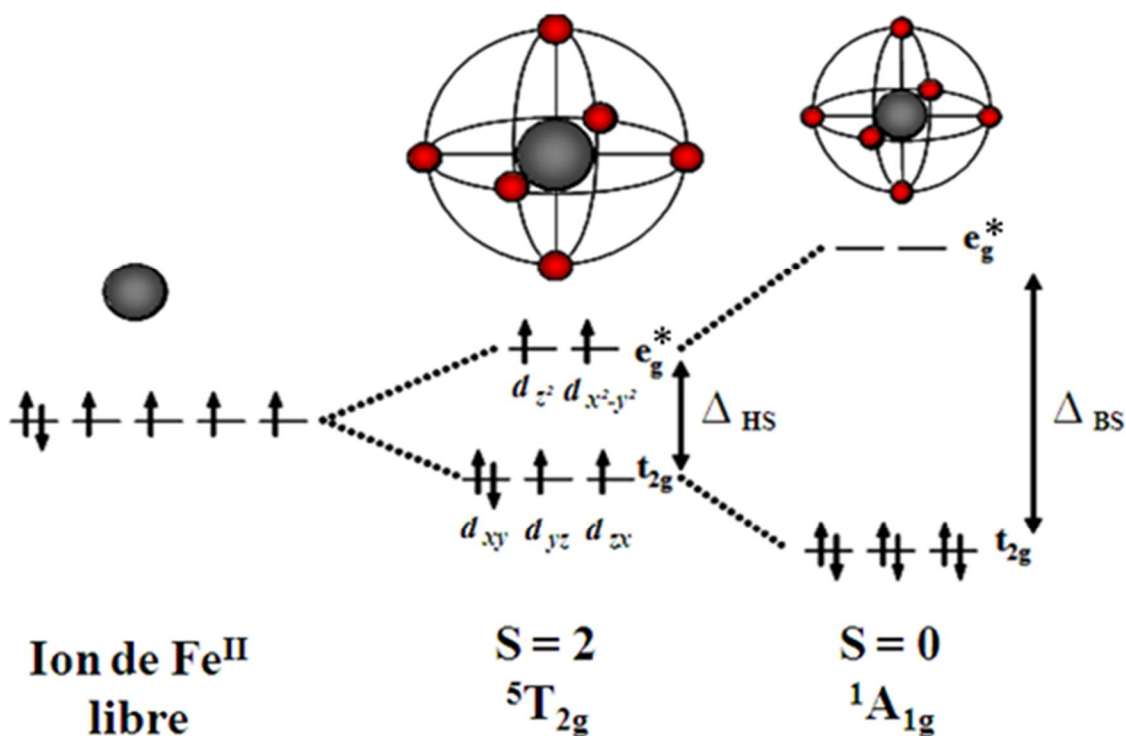
Figure 1.1. Degeneracy level and the electronic configuration of the HS and the LS state for the case of a Fe^{II} octahedral complex.

The change in spin state can be induced by various stimuli like temperature variation, pressure, light irradiation, magnetic field, or electric field, however the most common way to detect spin transition is by temperature variation. A spin transition curve plotted as high spin fraction γ_{HS} vs. temperature can provide plenty of information depending on its shape. Typical behaviors include gradual, abrupt (with or without hysteresis) and stepped spin crossover. Diverse experimental techniques can be used to monitor the spin state of the material: optical reflectivity measurements, magnetic measurements, calorimetric measurements, spectroscopic and crystallographic investigations etc.

1.2 State of the art in charge transport and electrical properties of SCO materials

Starting from the pioneering works on the bistability of the dielectric constant of bulk SCO powders to the voltage-triggered spin transition in a single molecule, this field has advanced

considerably in the past decade. At the macroscopic scale the spin-state dependence of charge transport and dielectric properties offers new opportunities for the investigation of the charge carrier dynamics and electronic structure of these compounds. In addition, these properties open up perspectives for the development of micro- and nano-electronic devices with spin-state switching functionality. The highly insulating nature of SCO compounds represent, however, an obstacle for a number of applications. This problem has been overcome by the development of hybrid SCO-conductor systems, which provide in addition also interesting synergy between different electronic phenomena. Hybrid materials were first synthesized by the co-crystallization of molecular SCO and conductor units, which proved to be a fundamentally very interesting, but also very challenging synthetic task. In a more pragmatic manner, SCO complexes were also mixed with piezoresistive polymers, which lead eventually to bistable conducting composite materials. Other possible approaches to overcome the insulating nature of SCO compounds are based on the device design (Figure 1.2.). For example devices with different competing charge transport channels can be constructed wherein the spin crossover phenomenon can lead to a switching in the nature of molecular orbitals involved in the charge carrier transport.
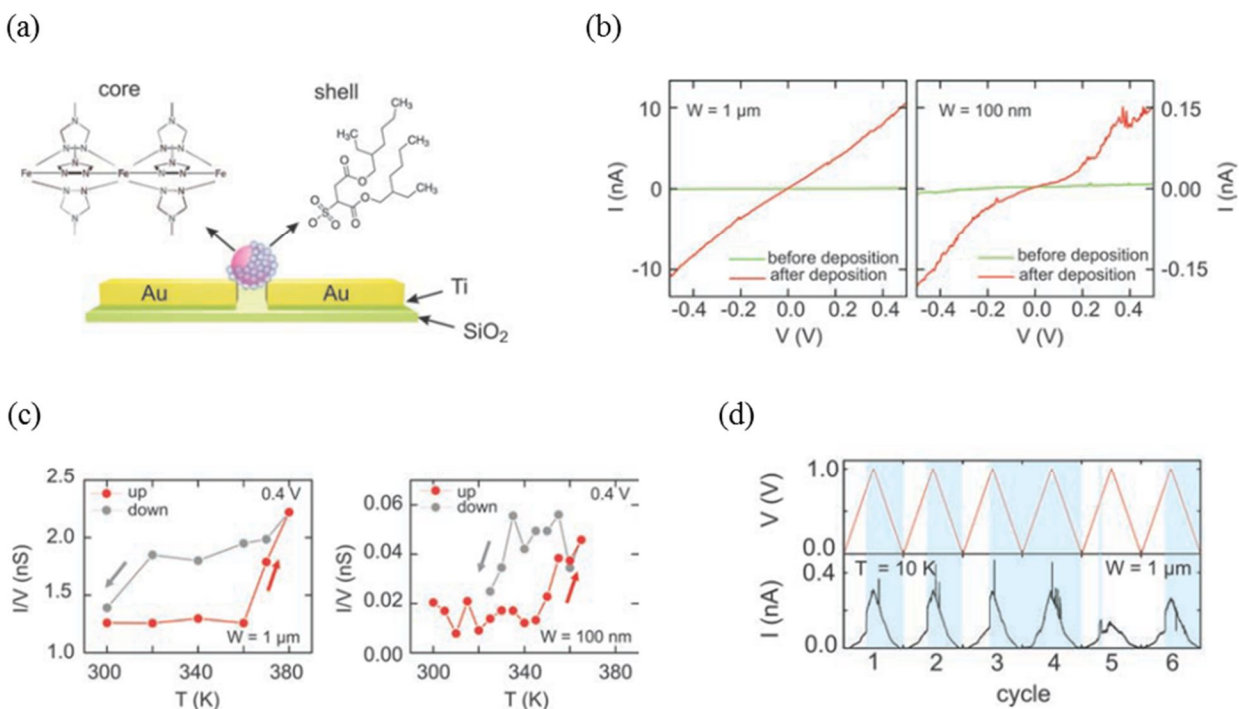
Figure 1.2. Schematic representation, current-voltage and current-temperature characteristics of a nanoelectronic device with [Fe(Htrz)$_2$(trz)](BF$_4$) particles in the electrode gap.

11

Another interesting possibility is the fabrication of tunneling devices with large area SCO tunnel junctions, which may open up also prospects for spintronic devices. Another field in fast development is the study of charge transport in SCO complexes at the single molecule level. In the case of single molecule devices, it has been shown that the coupling between the SCO molecule and the metallic electrode has a major impact on the electronic structure and switching properties of the molecule. Nevertheless, by carefully controlling this interface, remarkable results have been presented on single molecules or molecular clusters – including also their electrical addressing. Further work is, however, necessary to clarify the microscopic details of the different phenomena reported at the single molecule level.

Chapter 2: Electrical properties of spin crossover compounds in powder form

Electrical characterization of SCO materials is essential in understanding their behavior, and their potential applications in micro/nanoelectronic devices. In this chapter the quasi-static and dynamic electrical properties of the $[Fe(Htrz)_2(trz)](BF_4)$ spin crossover complex and its Zn diluted analogues ($[Fe_{1-x}Zn_x(Htrz)_2(trz)](BF_4)$ were studied using broadband dielectric spectroscopy.

In the first part of this chapter, an unprecedented behavior of the complex permittivity upon the spin transition in the compound $[Fe(Htrz)_2(trz)](BF_4)$ was reported (Figure 2.1). It has been shown that the dielectric relaxation frequency is strongly dependent on the spin state of the complex, denoting different relaxation mechanisms, which could be related to the structural changes (lattice deformation) between the two spin states. The AC and DC conductivity, as well as the dielectric constant and the dielectric relaxation frequency exhibit a spin state dependence, with an important drop when going from the LS to the HS state. All these measured quantities represent a different facet of the charge carrier dynamics, conferring unique properties to this material and making it interesting for threshold switching and memory devices as well as thermally variable capacitors due to their hysteresis in the conductivity as well as the dielectric constant.
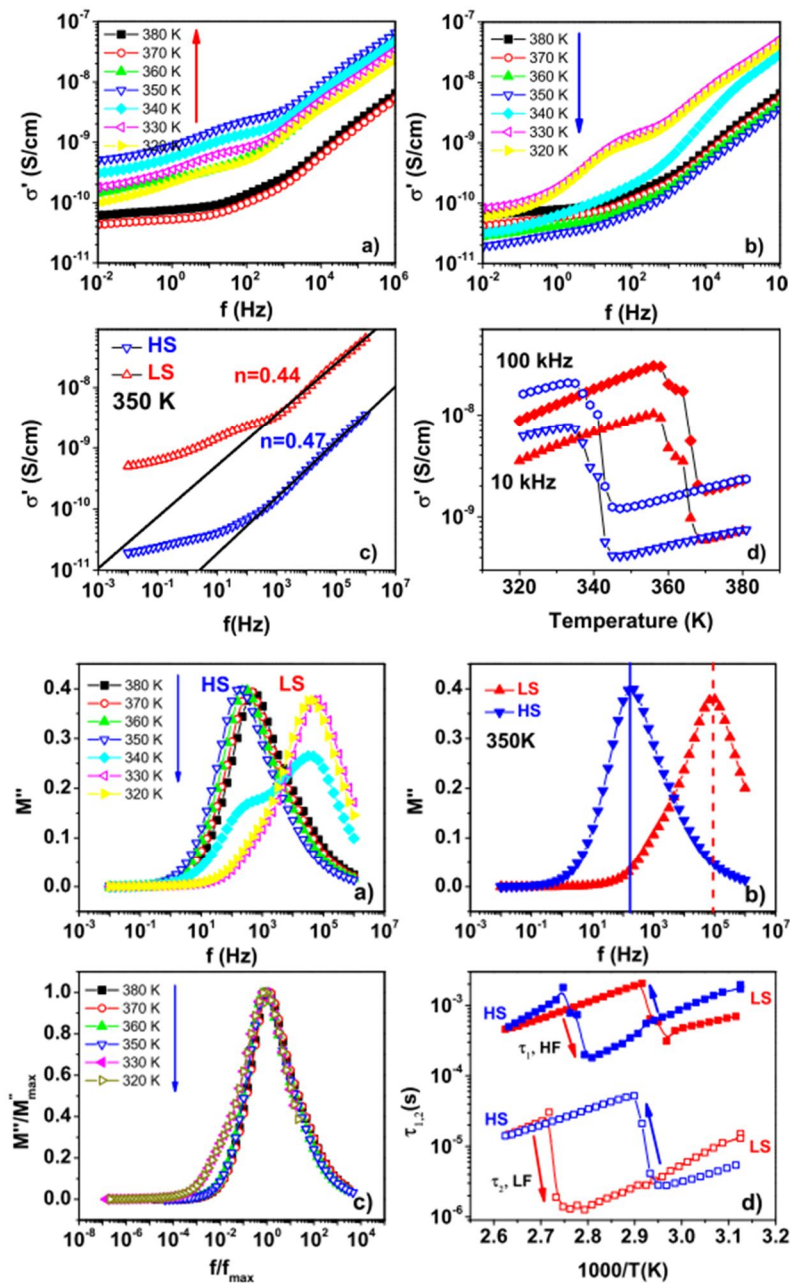
Figure 2.1 Top panel: Real part of the AC conductivity of the $[Fe(Htrz)_2(trz)](BF_4)$ as a function of the frequency, measured at selected temperatures in the (a) heating and (b) cooling modes. (c) Conductivity spectra at 350 K in the HS and LS states. The fits of the high-frequency part of the spectra are also shown. (d) Thermal hysteresis of σ' recorded at 10 kHz and 100 kHz. Bottom panel: (a) Dielectric loss modulus M" at selected temperatures in the cooling mode. (b) Spin state dependence of M" at 350 K. c) Plot of the normalized loss modulus ($M"/M"_{max}$) as a

function of the reduced frequency (f/f_{max}). d) Thermal hysteresis loops of the HN relaxation times ($\tau_{1,2}$).

The substitution of the "active" Fe centers by "inactive" Zn ions lead to some important findings concerning the charge transport properties of this spin crossover compound. The metal substitution was found homogeneous and the obtained compounds appeared closely isostructural. The iron ions kept their spin transition properties in the diluted samples, but as expected a loss of cooperativity and a shift of the spin transition towards lower temperatures was observed with increasing the iron dilution by zinc. It has been demonstrated that spin crossover phenomena can be also detected through the temperature dependence of AC conductivity and dielectric loss and show that virtually all material dependent electrical parameters, such as electrical conductivity, electric modulus, cut-off frequency, relaxation peak frequency, etc. display a spin-state dependence. In particular, it has been shown that the spin transition from the LS to the HS state led to a systematic decrease of the electrical conductivity and carrier hopping frequencies, which were related to the higher values of the activation energy in the HS state.
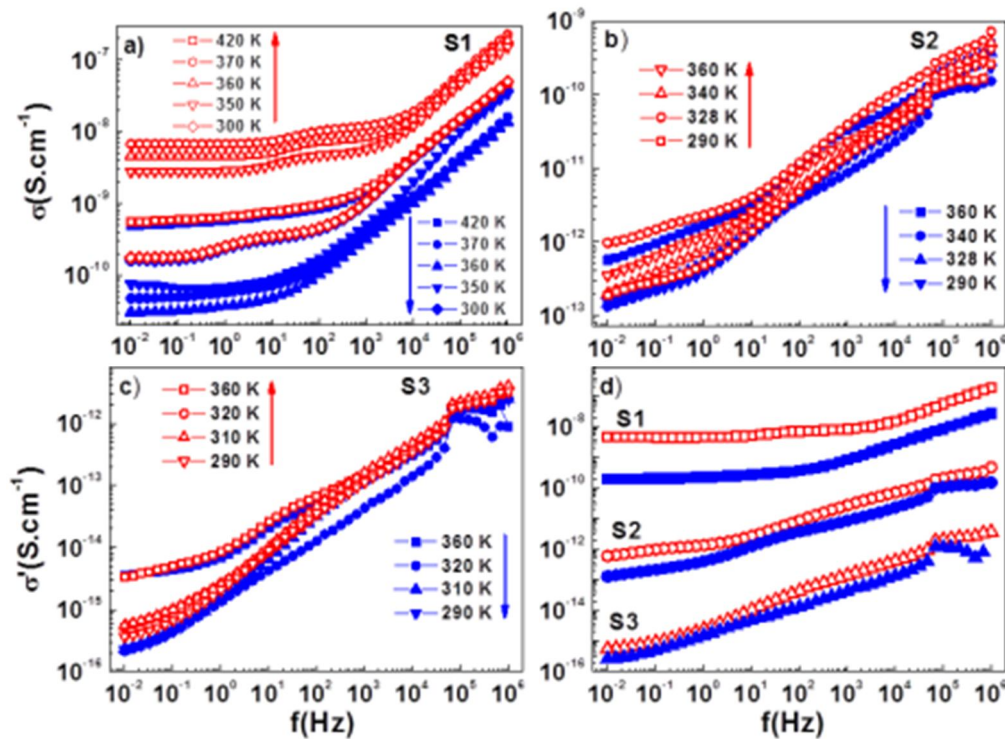
Figure 2.2. Frequency and temperature dependence of the AC conductivity for increasing Zn dilution: S1 < S2 < S3.

The Zn substitution of active iron centers do not change the activation barriers, but leads to an important decrease of the charge carrier hopping frequencies, which is reflected by the drop of the electrical conductivity by ca. 6 orders of magnitude (. Taking into account the close structural and morphological similarity of the pure and Zn-diluted samples these results indicate that the ferrous ions with open $3d^6$ electronic shell directly participate to the charge transport process, in contrast to the Zn(II) ions, which have a closed $3d^{10}$ shell.

Chapter 3: Elaboration and characterization of an electronic device in horizontal configuration containing [Fe(Htrz)$_2$(trz)](BF$_4$) particles

In this chapter we described the fabrication process and characterization of SCO based microelectronic devices obtained by performing dielectrophoresis on micrometric particles of the [Fe(Htrz)$_2$(trz)](BF$_4$) complex. We first determined the optimum parameters for organizing the particles between the interdigitated electrodes, which allowed us to obtain a dense and fairly uniform coverage of the interelectrode gaps by the particles. In agreement with previous results, in each device we observed a thermal hysteresis of the current intensity under applied bias, which we could clearly correlate with the spin transition. In agreement with the measurements on the bulk samples (see Chapter 2) the current flowing in the device is significantly higher in the low spin state of the complex. Then we performed an analysis of the stability of the spin transition for both the starting material and the device. It was shown that the particles keep their spin transition properties even after 3000 thermal switching cycles in ambient air, but the cooling branch of the hysteresis associated with the SCO shifts slowly to higher temperature (Figure 3.1).
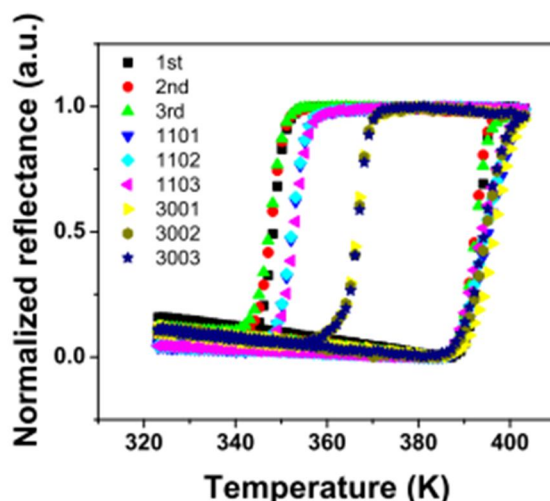
Figure 3.1. Thermal hysteresis of [Fe(Htrz)$_2$(trz)](BF$_4$) corresponding to the spin transition before and after 1100 and 3000 consecutive cycling.

Microelectronic devices were fabricated using dielectrophoresis on micrometric particles between interdigitated electrodes. The interdigitated gold microelectrodes were fabricated by conventional photolithography and liftoff techniques. Due to the fact that in our experiments the particle size was changed with respect to [25], the efficiency of dielectrophoresis was re-evaluated. The particles were dispersed in ethanol, obtaining a solution with a concentration of 2 g/L. The solution was dropcasted on the electrode and the electric field was applied through two gold tipped tungsten micro-probes from a signal generator. After 10 s the excess solution was removed and the electric field was interrupted. The optimal dielectrophoresis parameters were found (7.5 V_{RMS} at a frequency of 10 kHz) and use to obtain all the microelectronic devices presented further.
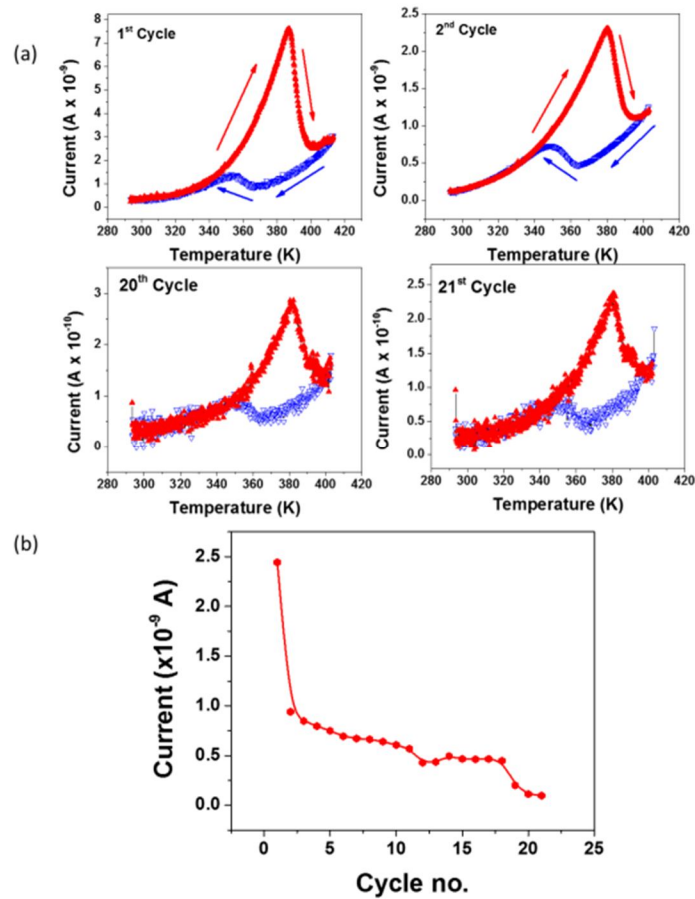
Figure 3.2 (a) Selected current vs. temperature characteristic of the electronic device of the device over consecutive thermal cycles. (b) Variation of the mean current intensity recorded in heating mode during 21 consecutive thermal cycles.

18

The I-T curve of the obtained micro-electronic device is presented in Figure 3.2a. The shape of the curve is similar to what it has been reported on a similar complex (C1 from ref [20]) and presents a strong thermally activated behavior with increasing temperature. The current increases exponentially from 0.3 nA to 7.6 nA at 387 K, where it drops abruptly at 2.5 nA at 402 K, which is a clear indication of the LS to HS transition. In the cooling mode, the current presents a slightly less thermal activation, and around 367 K the current starts increasing from 0.8 nA to 1.3 nA at 352 K, which is consistent with the HS to LS transition.

At the device level the spin transition appears also robust, but the current intensity decreases continuously upon thermal cycling (Figure 3.2b), which we tentatively attributed to a deterioration of the particle/particle and/or particle/electrode contacts. Further studies will be necessary to overcome this problem and obtain more robust devices. A possible approach would be the encapsulation of the device. We have also investigated the effect of light irradiation on these devices. By fixing the temperature inside the hysteresis loop in the low spin state, a reversible decrease in the current intensity as well as a slow irreversible increase of the current was observed under light irradiation (Figure 3.3). In the high spin state no effect could be detected in otherwise identical conditions (bias, temperature, light irradiation).
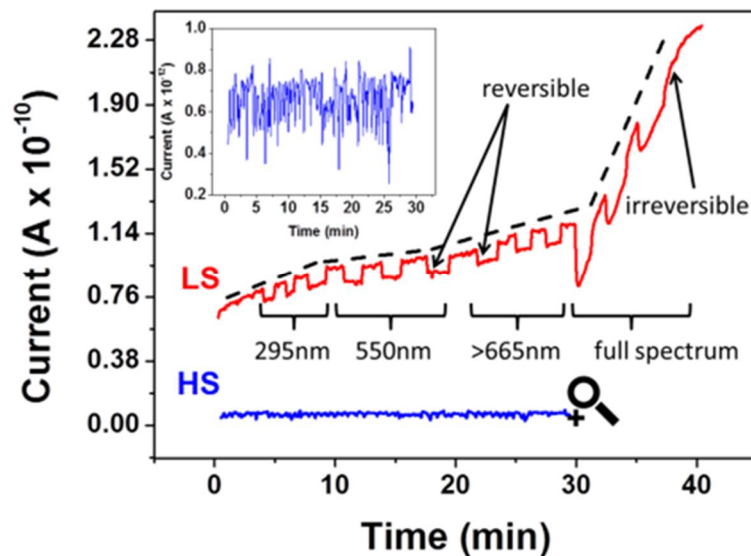

Figure 3.3. Current flowing in the device at 368 K under light irradiation at 20 V bias in air both in the HS and LS states. Light was successively turned on and off at different wavelengths as indicated in the figure.

These photoeffects seem to be related to the mobility of the charge carriers, which increases with increasing temperature and which is significantly higher in the low spin state of the material when compared to the high spin state. The observed light-induced phenomena are also related to some extent to the sample environment as the effects are more pronounced in the presence of oxygen and humidity. Moreover no correlation could be made with the absorption spectrum of the spin crossover compound. These two latter observations point to a possible adsorbate mediated redox mechanism behind the photoeffects. While the underlying mechanism needs further investigations, it is clear that this possibility of turning on and off the photoeffect by switching the spin state of the system (within the hysteresis loop) is a new and promising property of spin crossover devices, which broadens the scope of their future applications.

In the last part of this chapter, the electric field induced switching of the spin state of the $[Fe(Htrz)_2(trz)](BF_4)$ complex at the macroscopic scale is demonstrated. The unidirectional switching from the metastable HS to the stable LS state has been achieved by applying an electric field step inside the hysteresis loop (Figure 3.4). The field effects were discussed in the frame of the well-known static and dynamic Ising-like models. This approach allowed to reproduce qualitatively the main features of the experimental observations: stabilization of the LS state, slow and incomplete switching within the hysteresis due to the kinetic barriers.
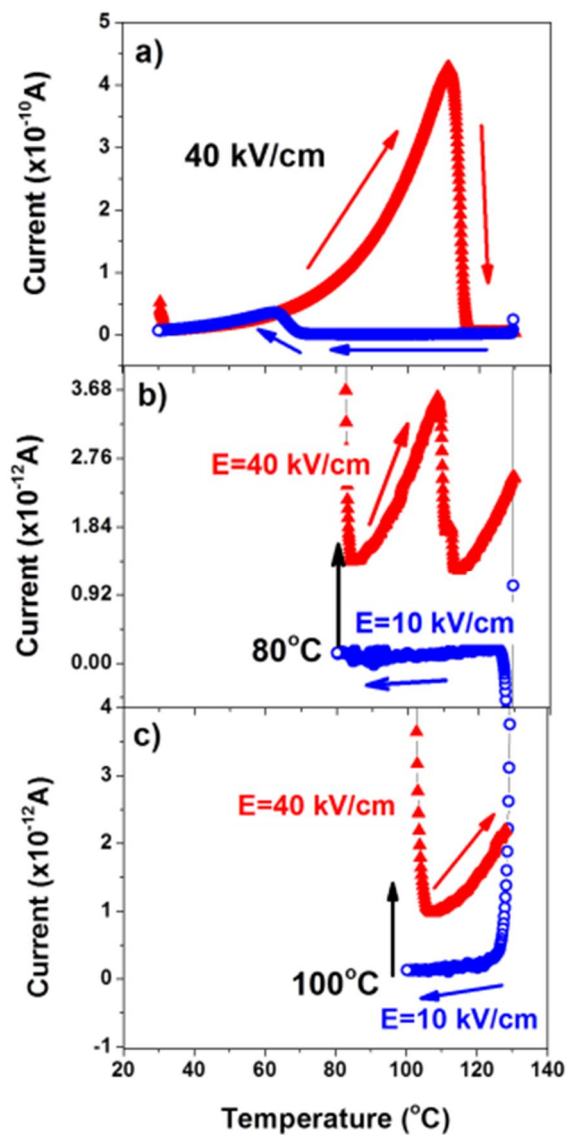
Figure 3.4. Current vs temperature characteristics of the interdigitated electrode device connected with particles of [Fe(Htrz)$_2$(trz)](BF$_4$). a) Full heating-cooling cycle between 30 and 130 °C under 40 kV/cm electric field. b-c) Incomplete thermal cycles: cooling from 130 to 80 °C (b) or to 100 °C (c) under 10 kV/cm bias followed by heating back to 130 °C under an electric field of 40 kV/cm.

Chapter 4: Elaboration and characterization of nanoelectronic devices in vertical configuration

This chapter describes an alternative approach for charge transport measurements in the tunneling regime based on robust, well-reproducible large-area vertical devices with thin SCO spacer layers (Figure 4.1). This approach allowed us to probe the spin-state switching in the SCO layer by optical means while detecting the associated resistance changes both in the tunneling (thin junction) and injection-limited (thick junction) regimes. The high current intensity in the devices provided also possibility for mechanistic studies by means of temperature- and frequency-dependent dielectric spectroscopy.
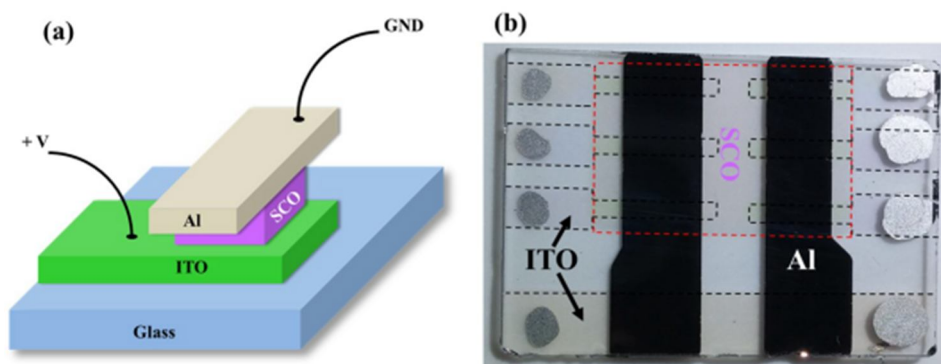
Figure 4.1 Device structure. (a) Schematic representation of the ITO/SCO/Al junction. (b) Photograph of a device with six crossbar junctions. The regions with ITO and SCO films are indicated by dashed lines. Silver paste contacts on the ITO are also visible.

Obviously, the main bottleneck to this approach is the need for high quality, ultrathin, pinhole-free SCO films over large electrode areas, which resist also to the deposition of the upper metallic electrode. To this aim the $[Fe(bpz)_2(phen)]$ SCO complex has been chosen (bpz = dihydrobis(pyrazolyl)borate and phen = 1,10-phenantroline), which is one of the scarce SCO compounds that can be deposited by thermal evaporation. The bulk powder of $[Fe(bpz)_2(phen)]$ displays a rather abrupt spin transition, with a very narrow hysteresis, while the vacuum-deposited films exhibit a gradual spin crossover (Figure 4.2). Both the powder and film samples

are known to exhibit also light-induced excited spin-state trapping (LIESST) phenomenon below ca. 50 K. Interestingly, the spin crossover properties of the films are virtually independent of the film thickness from (at least) 1 µm down to the sub-monolayer (i.e. isolated molecule) level, which makes this material ideal for nanoelectronic devices. The fabricated devices have been studied in variable temperature DC and AC regimes as well as isothermally at 5 K, while attempting to observe the LIESST effect in electrical properties.
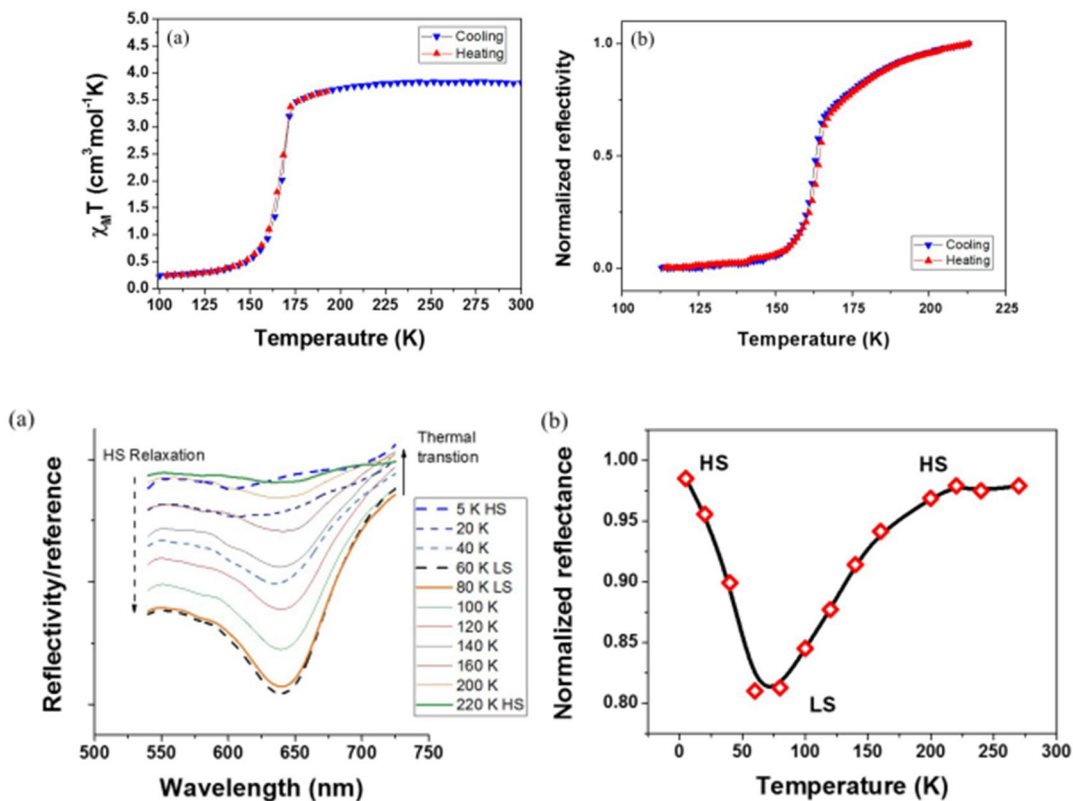
Figure 4.2 Top panel. Variable-temperature (a) magnetic susceptibility and (b) optical reflectivity of [Fe(bpz)$_2$(phen)] powder. Bottom panel: (a) Variable temperature reflectivity spectra for a glass/SCO/Al stack. (b) Temperature dependence of the optical reflectivity (λ=640 nm).

The devices with 10 nm junctions display tunneling conductivity (Figure 4.3), while the 100 nm junctions exhibit diode characteristics in a broad temperature range. The 30 nm devices show intermediate behavior: tunneling at low T and rectification at high T (Figure 4.4). Experimental

evidence that the spin-state switching of the junctions in the tunneling regime leads to a substantial and reversible increase/decrease of the tunneling current (up to 50 %) in the LS/HS states and we correlated this effect with the change of carrier hopping frequencies and distances upon the SCO is also provided.
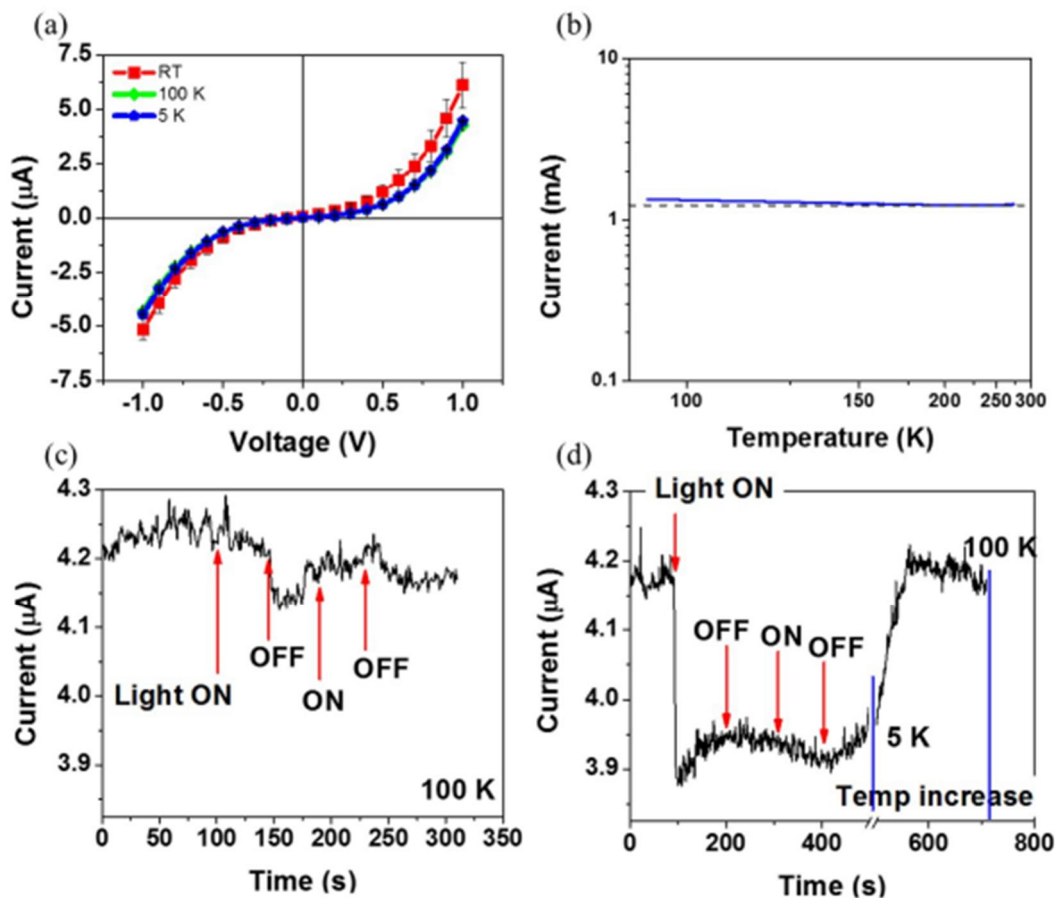
Figure 4.3. Electrical characteristics of a 10 nm junction. (a) I-V curves registered at room temperature, 100 K and 5 K. (b) Temperature dependence of the conductivity of the junction. (c) Visible light irradiation effect on the current flowing in the junction at 5 K followed by heating from 5 K to 100 K in the dark. (d) Visible light irradiation effect on the current flowing in the junction at 100 K.

In the injection regime no effect of the SCO on the device characteristics could be observed, however this might be simply masked by the intrinsic properties of these junctions. Overall these results provide very promising perspectives for using spin crossover compounds in electronic

devices. In addition, since the magnetic properties of the junction change also upon the SCO (diamagnetic vs. paramagnetic) even more appealing prospects appear for spintronic applications. Taking into account the current state of the art of the SCO field it is clear that there is no fundamental obstacle to prepare nanometric junctions with SCO compounds exhibiting room temperature switching properties. On the other hand, the technical challenge is substantial as it will be necessary to develop methods for the deposition of pinhole free films of these compounds between large area magnetic electrodes in a robust, reproducible way.
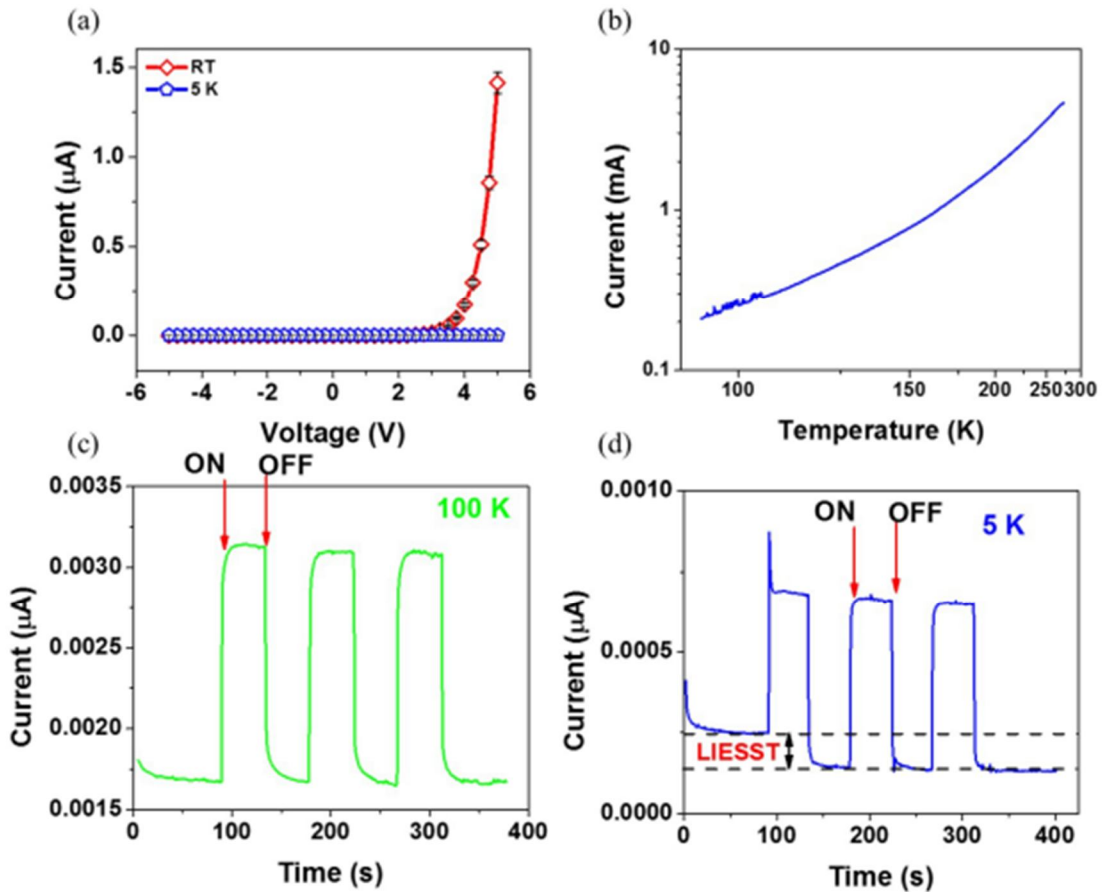

Figure 4.4. Electrical characteristics of a 30 nm junction. (a) I-V curves registered at room temperature and 5 K. b) Temperature dependence of the conductivity of the junction. (c-d) Visible light irradiation effect on the current flowing in the junction at 5 K (c) and 100 K (d).

General conclusions

The research presented in this thesis was motivated by the increasing interest of researchers in the development and study of spin crossover material based applications. These materials possess intriguing characteristics, the most important being molecular switching and hysteresis at nanometer level. These properties along with fast switching, sensitivity to different external stimuli and material design flexibility make these compounds suitable for various applications such as sensors, displays, memory or switching devices. During the last decade several prototypes and proofs of concept for various devices containing SCO materials have been proposed. However, reports of devices controlled by electrical signals are scarce. This might be a consequence of the rather limited understanding of the electrical properties of these materials, even though there are several remarkable studies on this topic. Starting from this state of the art, this thesis aimed for analyzing some interesting electrical properties of a few selected SCO materials from an experimental point of view.

In a first time we have investigated the benchmark spin crossover complex [Fe(Htrz)$_2$(trz)](BF$_4$) in the bulk powder form using broadband dielectric spectroscopy. We confirmed the rather low value (ca. 10^{-9} S/cm at 293 K) of its DC conductivity and showed that the previously reported drop of the DC conductance upon switching the complex from the LS to the HS state is also observable in the AC conductance within a broad frequency range (1 Hz – 1 MHz). The electric modulus formalism has been used to characterize the charge transport mechanism. In particular this approach revealed the co-existence of two distinct dielectric relaxation peaks at the same temperature corresponding to the two different spin states. The higher dielectric relaxation frequencies in the LS state suggest that the increase of the conductivity in this spin state occurs due to a higher charge carrier (polaron) hopping rate. We believe this will be the general trend for most SCO compounds since the hopping frequencies are strongly related to the mass density and the phonon frequencies of the material, which change in a similar manner in different SCO complexes. The electrical properties of the solid solutions [Fe$_{1-x}$Zn$_x$(Htrz)$_2$(trz)](BF$_4$) (x = 0, 0.26 and 0.43) were then investigated in the next step in order to determine the influence of the substitution of the "active" iron center by the "inactive" zinc ion. The physico-chemical analysis revealed that the obtained powder samples were closely isostructural and the Zn dilution was

homogeneous throughout the particles (of similar morphology), which are the necessary conditions for a pertinent comparison of their charge transport properties. Broadband dielectric spectroscopy revealed a considerable decrease in the electrical conductivity by ca. 6 orders of magnitude for the highest dilution as well as a shift of the spin transition towards lower temperatures and a shrinking of the hysteresis width. While the two latter phenomena were quite predictable, the drop of the conductivity is a remarkable new result as it proves that the iron ions participate directly in the charge transport process.

Using the $[Fe(Htrz)_2(trz)](BF_4)$ sample, microelectronic devices have been also fabricated by dielectrophoresis. The resulting devices were tested by electrical means, revealing a clear and reproducible spin state dependency of the measured current. While the spin transition in the starting powder could withstand 3000 thermal spin-state switching cycles (with a slow shrinking of the hysteresis width), at the device level a significant drop of the current intensity was observed after each cycle. This has been tentatively attributed to a degradation of the electrical contacts between the particles and the gold electrodes. These devices were then used to investigate the influence of different external stimuli, such as temperature, applied bias, light irradiation and environmental effects (presence of humidity and oxygen). Significant photoeffects on the current intensity were observed in the LS state of the device. This phenomenon could be correlated with the mobility of the charge carriers, which is significantly higher in the low spin state of the material when compared to the high spin state. The observed light-induced phenomena are also related to some extent to the sample environment as the effects were more pronounced in the presence of oxygen and humidity, suggesting a surface-mediated photochemical process at its origin. The most promising result on these devices was the successful switch from the HS to LS state by means of an applied electric field. This is the first report of spin state switching using an electric field to induce the spin transition at the macroscopic scale. Nevertheless the spin conversion obtained by applying and external electric field on this scale remains rather low (5 % at best). The switch has been performed inside the hysteresis loop near the cooling branch of the hysteresis, which discards the possibility that the observed effects are thermally induced. The effect of the electric field has been reproduced qualitatively using a modified Ising-like model wherein the dielectric permittivity difference between the HS and LS complexes was considered as the main ingredient for the field effect.

Nanoelectronic devices were also fabricated using the [Fe(bpz)$_2$(phen)] SCO complex, which was deposited by thermal evaporation between vertical electrodes. This way we could fabricate well reproducible devices with pinhole-free, large area SCO junctions of ca 10, 30 and 100 nm thickness. The thermal and light induced spin state switching in the devices was confirmed by optical means and correlated with the electrical characteristics. The charge transport mechanism in these devices was thickness dependent: temperature-independent tunneling for the 10 nm device and thermally activated, injection-limited conductance for the 100 nm device. The 30 nm device exhibited intermediate characteristics: diode-like rectification at high temperatures and tunneling behavior at low temperatures. The photo-induced spin-state switching effect on the device current has been clearly observed in the tunneling regime for the 10 nm and 30 nm devices, with the LS junction being more conducting (up to 50 % higher than the HS junction). We suggested the lower tunneling current in the HS state may be related to the reduced hopping rate of charge carriers. In the case of the rectifying junctions (30 - 100 nm) no obvious effect of the SCO on the electrical characteristics could be evidenced despite compelling theoretical predictions. It is possible, however, that the SCO effect on the current intensity was masked by the intrinsic sensitivity of these devices to temperature changes as well as to light irradiation.

Overall the results obtained in this thesis highlight that molecular spin crossover materials can be incorporated in various micro and nanoelectronic devices in a rather straightforward manner allowing for a reversible modulation of device electrical characteristics by means of spin-state switching of the metal complexes. From a fundamental point of view, further studies, including experimental as well as theoretical approaches, will be necessary to obtain more insights into the relationship between the molecular structure and electrical properties of these compounds. Density functional theory (DFT) calculations may be particularly useful to this aim. Concerning the potential applications, the vertical junction devices we developed appear very promising. In particular, magneto-transport studies of these devices represent an exciting perspective due to the concomitant change of their electrical and magnetic characteristics. For further progress in this direction, it would be necessary to fabricate thin junctions exhibiting SCO around room temperature. A thorough investigation of the molecular orbitals involved in the charge transport process will be also indispensable using both theoretical (DFT) and experimental (voltammetry, photoelectron spectroscopy) methods.

Result dissemination

[1] **Lefter, C.**; Gural'skiy, I.y.A.; Peng, H.; Moln´ar, G.; Salmon, L.; Rotaru, A.; Bousseksou, A.; Demont, P. *"Dielectric and charge transport properties of the spin crossover complex [Fe(Htrz)2(trz)](BF4)"*, **Physica status solidi (RRL) Rapid Research Letters** 2014, **8**, 191-193.

[2] **Lefter, C.**; Tricard, S.; Peng, H.; Moln´ar, G.; Salmon, L.; Demont, P.; Rotaru, A.; Bousseksou, A. *"Metal substitution effects on the charge transport and spin crossover properties of [Fe1xZnx(Htrz)2(trz)](BF4) (trz = triazole)"*, **Journal of Physical Chemistry C** 2015, **119**, 8522-8529.

[3] **Lefter, C.**; Tan, R.; Dugay, J.; Tricard, S.; Moln´ar, G.; Salmon, L.; Carrey, J.; Rotaru, A.; Bousseksou, A. *"Light induced modulation of charge transport phenomena across the bistability region in [Fe(Htrz)$_2$(trz)](BF$_4$) spin crossover micro-rods"*. **Physical Chemistry Chemical Physics** 2015, **17**, 5151-5154.

[4] **Lefter, C.**; Tan, R.; Tricard, S.; Dugay, J.; Moln´ar, G.; Salmon, L.; Carrey, J.; Rotaru, A.; Bousseksou, A. *"On the stability of spin crossover materials: From bulk samples to electronic devices"*, **Polyhedron** 2015, 102, 434-440.

[5] **Lefter, C.**; Tan, R.; Dugay, J.; Tricard, S.; Moln´ar, G.; Salmon, L.; Carrey, J.; Nicolazzi, W.; Rotaru, A.; Bousseksou, A. *"Unidirectional electric field-induced spin-state switching in spin crossover based microelectronic devices"*, **Chemical Physics Letters**, 2015, **644**, 138-141, *(Editor's Choice article).*

[6] **Lefter, C.**; Davesne, V.; Salmon, L.; Moln´ar, G.; Demont, P.; Rotaru, A.; Bousseksou, A. *"Charge transport and electrical properties of spin crossover materials: towards nanoelectronic and spintronic devices"*. **Magnetochemistry**, Special Issue "Spin Crossover (SCO) Research" - Review, submitted.

[7] **Lefter, C.**; Rat, S.; Costa, J.S.; Manrique-Juarez, M.D.; Quintero, C.; Salmon, L.; Molnar, G.; Seguy, I.; Nicu, L.; Demont, P.; Rotaru, A.; Bousseksou, A., *"Molecular spin-state switching in large-area vertical tunnel junctions"*, **Advanced Materials**, submitted 2016.

Selective Bibliography

[1]   P. Gutlich, H.A. Goodwin, Topics in Current Chemistry. *Spin Crossover in Transition Metal Compounds I.*, Springer-Verlag, Berlin, 2004.

[2]   P. Gutlich, A. Hauser, H. Spiering, *Angewandte Chemie-International Edition,* **33** (1994) 2024.

[3]   A. Bousseksou, G. Molnar, L. Salmon, W. Nicolazzi, *Chemical Society Reviews* **40** (2011) 3313.

[4]   H. Spiering, *Spin Crossover in Transition Metal Compounds III*, 2004, p. 171.

[5]   J.K. McCusker, K.N. Walda, R.C. Dunn, J.D. Simon, D. Magde, D.N. Hendrickson, *Journal of the American Chemical Society* **114** (1992) 6919.

[6]   J.F. Letard, P. Guionneau, L. Goux-Capes, *Spin Crossover in Transition Metal Compounds III*, 2004, p. 221.

[7]   O. Kahn, C.J. Martinez, *Science* **279** (1998) 44.

[8]   J. Linares, E. Codjovi, Y. Garcia, *Sensors* **12** (2012) 4479.

[9]   C. Bartual-Murgui, A. Akou, C. Thibault, G. Molnar, C. Vieu, L. Salmon, A. Bousseksou, *Journal of Materials Chemistry C* **3** (2015) 1277.

[10]   L. Salmon, G. Molnar, D. Zitouni, C. Quintero, C. Bergaud, J.C. Micheau, A. Bousseksou, *Journal of Materials Chemistry* **20** (2010) 5499.

[11]   M. Matsuda, K. Kiyoshima, R. Uchida, N. Kinoshita, H. Tajima, *Thin Solid Films* **531** (2013) 451.

[12]   H.J. Shepherd, I.y.A. Gural'skiy, C.M. Quintero, S. Tricard, L. Salmon, G. Molnár, A. Bousseksou, *Nat Commun* **4** (2013).

[13]   A. Bousseksou, G. Molnar, *Comptes Rendus Chimie* **6** (2003) 1175.

[14]   S. Bonhommeau, T. Guillon, L.M.L. Daku, P. Demont, J.S. Costa, J.F. Letard, G. Molnar, A. Bousseksou, *Angewandte Chemie-International Edition* **45** (2006) 1625.

[15]   C. Faulmann, K. Jacob, S. Dorbes, S. Lampert, I. Malfant, M.L. Doublet, L. Valade, J.A. Real, *Inorganic Chemistry* **46** (2007) 8548.

[16]   K. Takahashi, H.B. Cui, Y. Okano, H. Kobayashi, Y. Einaga, O. Sato, *Inorganic Chemistry* **45** (2006) 5739.

[17] M. Nihei, N. Takahashi, H. Nishikawa, H. Oshio, *Dalton Transactions* **40** (2011) 2154.

[18] L. Salmon, G. Molnar, S. Cobo, P. Oulie, M. Etienne, T. Mahfoud, P. Demont, A. Eguchi, H. Watanabe, K. Tanakae, A. Bousseksou, *New Journal of Chemistry* **33** (2009) 1283.

[19] T. Mahfoud, G. Molnar, S. Cobo, L. Salmon, C. Thibault, C. Vieu, P. Demont, A. Bousseksou, *Applied Physics Letters* **99** (2011).

[20] A. Rotaru, I.y.A. Gural'skiy, G. Molnar, L. Salmon, P. Demont, A. Bousseksou, *Chemical Communications* **48** (2012) 4163.

[21] C. Etrillard, V. Faramarzi, J.-F. Dayen, J.-F. Letard, B. Doudin, *Chemical Communications* **47** (2011) 9663.

[22] M.S. Alam, M. Stocker, K. Gieb, P. Muller, M. Haryono, K. Student, A. Grohmann, *Angewandte Chemie-International Edition* **49** (2010) 1159.

[23] V. Meded, A. Bagrets, K. Fink, R. Chandrasekar, M. Ruben, F. Evers, A. Bernand-Mantel, J.S. Seldenthuis, A. Beukman, H.S.J. van der Zant, *Physical Review B* **83** (2011) 245415.

[24] F. Prins, M. Monrabal-Capilla, E.A. Osorio, E. Coronado, H.S.J. van der Zant, *Advanced Materials* **23** (2011) 1545.

[25] A. Rotaru, J. Dugay, R.P. Tan, I.y.A. Gural'skiy, L. Salmon, P. Demont, J. Carrey, G. Molnar, M. Respaud, A. Bousseksou, *Advanced Materials* **25** (2013) 1745.